Applied Mathematics and Computation 321 (2018) 176–194

Contents lists available at ScienceDirect

Applied Mathematics and Computation

journal homepage: www.elsevier.com/locate/amc

A data assimilation approach for non-Newtonian blood flow simulations in 3D geometries

Telma Guerra[a,b], Catarina Catarino[c,1], Tânia Mestre[c,1], Sara Santos[c,1], Jorge Tiago[b,*], Adélia Sequeira[b]

[a] Escola Superior de Tecnologia do Barreiro, Instituto Politécnico de Setúbal, Rua Américo da Silva Marinho, Lavradio 2839–001, Portugal
[b] CEMAT, Instituto Superior Técnico, Universidade de Lisboa, Av. Rovisco Pais, Lisboa 1049–001, Portugal
[c] Instituto Superior Técnico, Universidade de Lisboa, Av. Rovisco Pais, Lisboa 1049–001, Portugal

ARTICLE INFO

Keywords:
Optimal control
Non-Newtonian fluids
Data assimilation

ABSTRACT

Blood flow simulations can play an important role in medical training and diagnostic predictions associated to several pathologies of the cardiovascular system. The main challenge, at the present stage, is to obtain reliable numerical simulations in the particular districts of the cardiovascular system that we are interested in. Here, we propose a Data Assimilation procedure, in the form of a non linear optimal control problem of Dirichlet type, to reconstruct the blood flow profile from known data, available in certain parts of the computational domain. This method will allow us to obtain the boundary conditions, not fully determined by the physics of the model, in order to recover more accurate simulations. To solve the control problem we propose a Discretize then Optimize (DO) approach, based on a stabilized finite element method. Numerical simulations on 3D geometries are performed to validate this procedure. In particular, we consider some idealized geometries of interest, and real geometries such as a saccular aneurysm and a bypass. We assume blood as an homogeneous fluid with non-Newtonian inelastic shear-thinning behavior. The results show that, even in the presence of noisy data, accuracy can be improved using the optimal control approach.

© 2017 Elsevier Inc. All rights reserved.

1. Introduction

The increasing collaboration between scientists working in multidisciplinary areas such as medical researchers and clinicians, mathematicians and bioengineers has contributed to data information exchange that can be used in the numerical simulations providing more realistic results and increasing the advantages in therapy prediction and surgical planning.

The techniques based on the inclusion of data measurements in the numerical simulations are known, in the literature, as Data Assimilation (DA). Such techniques have already been used in other engineering fields like geophysics and meteorology (for an overview, see [40] and the references therein). More recently, DA variational approaches were also used to improve blood flow simulations [18,24]. Besides, techniques based on the unscented Kalman filter were suggested to perform parameter estimation in cardiovascular modeling (see [7,32,34] and [31] for an overview).

* Corresponding author.
E-mail address: jftiago@math.tecnico.ulisboa.pt (J. Tiago).
[1] These authors contributed equally to this work.

https://doi.org/10.1016/j.amc.2017.10.029
0096-3003/© 2017 Elsevier Inc. All rights reserved.

In [18], several approaches were compared, namely the domain splitting method, the matrix updating technique and the variational approach. The later was shown to give the best results among the three techniques. This approach consists in minimizing the misfit between the observed data and the solution of the model, by controlling certain free parameters. The authors assumed the viscosity function in (1) to be constant, and took the value of the pressure on the inlet boundary as the parameter to control. In [24] this approach was reformulated to include the possibility of controlling the velocity profile itself. The authors performed a parameter fitting for the cost function and verified the robustness of the approach, with respect to noise reduction, in a 2D idealized stenosis. In [38], the authors used DA techniques as a tool for improving the accuracy of computational domains reconstructed from medical images. The existence of solution for these mathematical approaches to the DA problem was not established yet. However, numerical solutions based on a Discretized then Optimize (DO) approach was shown to be successful in this frame. The DO consists in first discretizing the variational (optimal control) problem describing the DA method, and then solving the resulting nonlinear finite-dimensional optimization problem. The DO approach is often put side by side with the Optimize then Discretize (OD) approach, but it is not clear yet which is the most suitable in the frame of fluid control. For example, in [8] and [29], it is indicated that, for certain kinds of parabolic problems, a DO approach is preferred. For fluid control problems the authors show that the discrete solution may not converge to the solution of the continuous problem while using OD. Conversely, in [16], it is shown that, in certain cases of stabilized advection equations, the OD has better asymptotic convergence properties. For more details on this issue see, [11,18,25], or [28].

In this paper we propose a DA technique to control the velocity inlet profile in 3D domains. As a first approach, the model is assumed to be stationary, in order to neglect the fluid interaction with the vessel walls. This assumption allows to consider the modeling of some pathologies for which only a long term blood flow profile is required. One of such pathologies is atherosclerosis, one of the deadliest cardiovascular diseases. For such large time scales, it becomes unreasonable to model the short scale pulsatile effects. In future work, we should consider the assimilation of space dependent data obtained at different time steps. Dealing with time dependent data will allow to model clinical problems in which the pulsatile nature of blood is determinant. The methodology adopted includes the use of the Sequential Quadratic Programming method [19] to solve the discretized optimization problem. The result is a large scale finite dimensional, nonlinear optimization problem. Here, we investigate the robustness of this approach in such cases. Therefore, we consider different idealized and realistic geometries. The later represent particular districts of the arterial system, under pathological stages, which were obtained from medical images. We assess the robustness of the method in such domains and analyze the influence of the location of data measurements.

This paper is organized as follows. In Section 2 we introduce the 3D blood flow mathematical model, considered as a shear-thinning non-Newtonian fluid, and we describe the variational approach for the DA problem. In Section 3 we show how to use the DO approach to solve the DA problem and describe the optimization algorithm. In Section 4, we present and discuss the numerical results obtained for different 3D geometries.

2. Data Assimilation approach

To outline the Data Assimilation procedure, we first describe the fluid flow equations as well as the viscosity model, used in the numerical simulations.

In this work we assume that blood is an incompressible, shear-thinning fluid at constant temperature. By fixing Ω as a 3D domain of interest, the equations describing the linear momentum and mass conservation, under the steady assumption, can be written as

$$\begin{cases} -div\,(\tau(D\mathbf{u})) + \rho(\mathbf{u}\cdot\nabla)\mathbf{u} + \nabla p = \mathbf{f} & \text{in } \Omega \\ div\,\mathbf{u} = 0 & \text{in } \Omega \end{cases} \tag{1}$$

complemented with suitable boundary and initial conditions. Here $\mathbf{u}$ refers to the velocity field and p to the pressure. The constant parameter ρ represents the density of the fluid and $\mathbf{f}$ the body force. The tensor of viscous stresses is represented by

$$\tau = 2\mu(\dot{\gamma})D\mathbf{u},$$

where μ is the dynamic viscosity, $\dot{\gamma}$ refers to the shear rate

$$\dot{\gamma} = \sqrt{\frac{1}{2}(\nabla\mathbf{u} + (\nabla\mathbf{u})^T) : (\nabla\mathbf{u} + (\nabla\mathbf{u})^T)} = \sqrt{2}|D\mathbf{u}|$$

and D represents the strain rate tensor

$$D\mathbf{u} = \frac{1}{2}\left(\nabla\mathbf{u} + (\nabla\mathbf{u})^T\right).$$

For a shear-thinning fluid we assume the viscosity to decrease with growing shear rate. Therefore, we assume μ to be given by

$$\mu(\dot{\gamma}) = \mu_\infty + (\mu_0 - \mu_\infty)F(\dot{\gamma}), \tag{2}$$

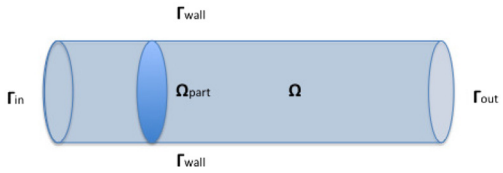


Fig. 1. Example of a three-dimensional domain Ω.

where $F(\dot\gamma)$ verifies

$$\lim_{\dot\gamma\to 0} F(\dot\gamma) = 1 \quad \text{and} \quad \lim_{\dot\gamma\to+\infty} F(\dot\gamma) = 0.$$

Hence, the viscosity ranges from μ_0, for null shear rates, and μ_∞ when $\dot\gamma$ goes to infinity.

Among the different possibilities for the choice of F [35], here we consider the generalized Cross and Carreau models corresponding to the functions

$$F(\dot\gamma) = \frac{1}{(1+(\lambda\dot\gamma)^b)^a}, \quad a, b, \lambda > 0$$

and

$$F(\dot\gamma) = (1+(\lambda\dot\gamma)^2)^{\frac{n-1}{2}}, \quad \lambda > 0, \quad 0 < n < 1,$$

respectively.

As mentioned above, Data Assimilation consists in using available data to reconstruct or improve the numerical solution of a given model, that should match the data at the locations where they were observed.

This work follows the DA approach proposed in [24] for the 2D case. The domain Ω represents part of an artery truncated by two artificial boundaries, the inlet and the outlet, which is represented by Γ_{in} and Γ_{out}, respectively. The artery wall is represented by Γ_{wall}. An example of such domain can be seen in Fig. 1. This approach consists in minimizing the cost functional

$$\mathbf{J}(\mathbf{u},\mathbf{g}) = w_1 \int_{\Omega_{\text{part}}} |\mathbf{u}-\mathbf{u}_d|^2\,dx + w_2 \int_{\Gamma_{in}} |\nabla\mathbf{g}|^2\,dx \tag{3}$$

subject to

$$\begin{cases} -div\,\tau(D\mathbf{u}) + \rho(\mathbf{u}\cdot\nabla)\mathbf{u} + \nabla p = \mathbf{f} & \text{in } \Omega \\ div\,\mathbf{u} = 0 & \text{in } \Omega \\ \mathbf{u} = 0 & \text{on } \Gamma_{\text{wall}} \\ \mathbf{u} = \mathbf{g} & \text{on } \Gamma_{\text{in}} \\ \sigma\cdot\mathbf{n} = 0 & \text{on } \Gamma_{\text{out}}. \end{cases} \tag{4}$$

The first term of J is the kernel term to be minimized: it measures the misfit between the solution $\mathbf{u}$ and the data $\mathbf{u}_d$ on the observed subdomain Ω_{part}. The second term is a regularizing term, that also adds some convexity to the cost function with respect to the dependence on the control parameter represented by $\mathbf{g}$, which is defined on Γ_{in}. Here σ represents the Cauchy stress tensor and $\mathbf{n}$ the unitary vector normal to the boundary surface. We assume that $\mathbf{w}_d$ is observed on the boundary represented by Γ_w.

To find the velocity profile $\mathbf{u}$ from (3)–(4), we close the system formed by momentum and mass conservation equations with a no slip condition on Γ_{wall} and a Neumann homogeneous condition on Γ_{out}.

Up to the authors knowledge, the existence of a solution to problem (3)–(4) has not been studied yet. A similar problem was treated in [23], for the Navier–Stokes equations. In the case of Generalized Newtonian fluids, existence results for related problems can be found in [2,14,15,22,27,37] and [39]. Unfortunately, none of those can be applied to problem (3)–(4). This implies that, at the present stage, we do not have information about the regularity of the solution. We will however assume that the solution is regular enough in order to allow a direct discretization of (3)–(4). This will be the subject of next section.

3. Numerical approximation

In this section, we describe the Discretize then Optimize (DO) approach applied to problem (3)–(4). Such approach consists in first discretizing the optimal control problem and then solving the finite dimensional optimization problem resulting from the discretization. We will now describe the first stage by considering the weak formulation of (1).

Let us assume that we are looking for $\mathbf{u} \in \mathbf{V} = \{\mathbf{u} \in \mathbf{H}^1(\Omega) : \ \mathbf{u}|_{\partial\Omega_D} = \mathbf{g}\}$ and $p \in \mathbf{Q} = \mathbf{L}^2(\Omega)$. We consider $\mathbf{V}_0 = \{\mathbf{v} \in \mathbf{H}^1(\Omega) : \ \mathbf{v}|_{\partial\Omega_D} = 0\}$, where $\partial\Omega_D = \Gamma_{\text{in}} \cup \Gamma_{\text{wall}}$, and $\mathbf{Q}$, as the spaces of test functions corresponding to $\mathbf{u}$ and p, respectively. The weak formulation of (1) can be formally obtained by multiplying both equations by suitable test functions and

integrating by parts, as follows

$$\begin{cases} \int_\Omega \tau(D\mathbf{u}) : \nabla \mathbf{v}\, dx + \int_\Omega (\rho(\mathbf{u}\cdot\nabla)\mathbf{u})\cdot\mathbf{v}\, dx - \int_\Omega p\, div\, \mathbf{v}\, dx = \int_\Omega \mathbf{f}\cdot\mathbf{v}\, dx \\ \int_\Omega q\, div\, \mathbf{u}\, dx = 0 \end{cases} \tag{5}$$

for all $\mathbf{v}\in\mathbf{V}_0$ and $q\in\mathbf{Q}$. The symbol ":" represents the inner product of two second-order tensors.

For the discretization of these equations we consider the finite dimensional approximations

$$\mathbf{u}_h = \sum_{j=1}^{N_u} u_j\phi_j \in \mathbf{V}_h, \quad p_h = \sum_{k=1}^{N_p} p_k\psi_k \in \mathbf{Q}_h \tag{6}$$

where u_j and p_k are unknown coefficients to be determined. Here, the finite dimensional space $\mathbf{Q}_h$ is a subspace of $\mathbf{Q}$, and is generated by the basis functions ψ_k, $k=1,\ldots,N_p$. The finite dimensional sets $\mathbf{V}_h$ and $\mathbf{V}_{0,h}$ are approximating subsets of $\mathbf{V}$ and $\mathbf{V}_0$, respectively. The shape functions ϕ_j, $j=1,\ldots,N_u$, belonging to $\mathbf{V}_h$, are an extension to $\partial\Omega_D$ of the basis functions spanning $\mathbf{V}_{0,h}$. In particular, we assume $\mathbf{V}_{0,\,h}$ and $\mathbf{Q}_h$ to represent Lagrange type Finite Elements spaces, associated to a partition $\mathcal{T}_h$ of $\overline{\Omega}$, where $h>0$ is the space index related to the space dimension. We refer to [3] and [4] for details on the numerical analysis of the finite element discretization of (5).

The problem becomes: find $\mathbf{u}_h\in\mathbf{V}_h$ and $p_h\in\mathbf{Q}_h$ such that

$$\begin{cases} \int_\Omega \tau(D\mathbf{u}_h) : \nabla\mathbf{v}_h\, dx + \int_\Omega (\rho(\mathbf{u}_h\cdot\nabla)\mathbf{u}_h)\cdot\mathbf{v}_h\, dx + \int_\Omega p_h\, div\, \mathbf{v}_h\, dx \\ = \int_\Omega \mathbf{f}\cdot\mathbf{v}_h\, dx, \quad \forall v_h\in V_{0,h} \\ \int_\Omega q_h\, div\, \mathbf{u}_h\, dx = 0, \quad \forall q_h\in Q_h. \end{cases} \tag{7}$$

To describe the approximated problem, we start by discretizing system (7). Since it is a convected dominated regime, a GLS (Galerkin–Least-Squares) stabilization is adopted. Let us consider the bilinear forms

$$a(\mathbf{u}_h,\mathbf{v}_h) = \int_\Omega \tau(D\mathbf{u}_h) : \nabla\mathbf{v}_h + \int_\Omega (\rho(\mathbf{u}_h\cdot\nabla)\mathbf{u}_h)\cdot\mathbf{v}_h + \int_\Omega p_h\, div\, \mathbf{v}_h$$

and

$$b(\mathbf{u}_h,q_h) = \int_\Omega q_h\, div\, \mathbf{u}_h.$$

Under this notation, the stabilization of system (7) consists in finding $\mathbf{u}_h\in\mathbf{V}_h$ and $p_h\in\mathbf{Q}_h$ by adding new terms $\mathcal{L}_h^1$ and $\mathcal{L}_h^2$ such that

$$\begin{cases} a(\mathbf{u}_h,\mathbf{v}_h) + \mathcal{L}_h^1(\mathbf{u}_h,\mathbf{f},\mathbf{v}_h) = (\mathbf{f},\mathbf{v}_h) \\ b(\mathbf{u}_h,q_h) = \mathcal{L}_h^2(p_h,q_h) \end{cases} \tag{8}$$

where

$$\mathcal{L}_h^1(\mathbf{u}_h,\mathbf{f},\mathbf{v}_h) = \sum_{K\in\tau_h} (L(\mathbf{u}_h,p_h) - \mathbf{f}, \varphi(\mathbf{u}_h,\mathbf{v}_h))$$

and

$$\mathcal{L}_h^2(p_h,q_h) = \left(-\frac{1}{\lambda}p_h, q_h\right).$$

Here, λ is a penalty parameter (see [10]) and L and φ are given by

$$L(\mathbf{u},p) = -div\,\tau(D(\mathbf{u})) + (\mathbf{u}\cdot\nabla)\mathbf{u} + \nabla p$$

$$\varphi(\mathbf{u}_h,\mathbf{v}_h) = \delta((\mathbf{u}_h\cdot\nabla)\mathbf{v}_h + div\,\tau(D(\mathbf{v}_h))).$$

The parameter δ should be suitably chosen. In this work, the parameter is taken from [5] (see [6] for more details). Notwithstanding, δ can be optimized in the frame of optimal control problems [16] and [1].

In order to discretize the system (8), let us look at the diffusion term of $a(\mathbf{y_h},\mathbf{v_h})$ and its counterpart in $\mathcal{L}_h^1(\mathbf{u}_h,\mathbf{f},\mathbf{v}_h)$

$$\int_\Omega \tau(D\mathbf{u}_h) : \nabla\mathbf{v}_h + \sum_{K\in\mathcal{T}_h}\int_K -div\,\tau(D\mathbf{u}_h)\cdot\varphi(\mathbf{u}_h,\mathbf{v}_h)$$

Replacing $\mathbf{v}_h$ by the extended basis ϕ_i, $i=1,\ldots,N_u$ and taking into account (6) we obtain (see [24]):

$$\left(\int_\Omega 2\mu\left(\left|\sum_{j=1}^{N_u} u_j D\phi_j\right|\right)\sum_{k=1}^{N_u} u_k D\phi_k : \nabla\phi_i\right)$$
$$+\sum_{K\in\mathcal{T}_h}\int_K -div\,\tau\left(D\left(\sum_{j=1}^{N_u} u_j D\phi_j\right)\right)\cdot\left(\delta\left(\sum_{i=1}^{N_u} u_i\phi_i\cdot\nabla\phi_i + div\,\tau(D(\phi_i))\right)\right)$$
$$=(Q+\mathcal{Q})(\mathbf{U}),\quad \forall i,j=1\dots N_u$$

Let us now focus on the convective term and its counterpart in $\mathcal{L}_h^1(\mathbf{u}_h,\mathbf{f},\mathbf{v}_h)$:

$$\int_\Omega((\mathbf{u}_h\cdot\nabla)\mathbf{u}_h)\cdot\mathbf{v}_h+\sum_{K\in\mathcal{T}_h}\int_K((\mathbf{u}_h\cdot\nabla)\mathbf{u}_h)\cdot\varphi(\mathbf{u}_h,\mathbf{v}_h).$$

Using the approximations (6) and after some computations, the above expression can be written as

$$\left(\sum_{j=1}^{N_u} u_j\sum_{k=1}^{N_u} u_k\int_\Omega(\phi_j\cdot\nabla)\phi_k\cdot\phi_i\right)_{i=1,\dots,N_u}$$
$$+\left(\sum_{K\in\tau_h}\sum_{j=1}^{N_u} u_j\sum_{k=1}^{N_u} u_k\int_K(\phi_j\cdot\nabla)\phi_k\cdot\left(\delta\left(\sum_{l=1}^{N_u} u_l\phi_l\cdot\nabla\phi_i+div\,\tau(D(\phi_i))\right)\right)\right)_{i=1,\dots,N_u}$$
$$=(N(\mathbf{U})+\mathcal{N}(\mathbf{U}))\mathbf{U}$$

where $\mathbf{U}=(u_1,\dots,u_{N_u})^T$ and $N(\mathbf{U})$ and $\mathcal{N}(\mathbf{U})$ are matrices whose elements are defined by

$$[N(\mathbf{U})]_{i,j}=\left(\sum_{k=1}^{N_u} u_k\int_\Omega(\phi_j\cdot\nabla)\phi_k\cdot\phi_i\right)\quad\forall\, i,j=1,\dots,N_u$$

$$[\mathcal{N}(\mathbf{U})]_{i,j}=\sum_{K\in\mathcal{T}_h}\sum_{k=1}^{N_u} u_k\int_\Omega(\phi_j\cdot\nabla)\phi_k\cdot\left(\delta\left(\sum_{l=1}^{N_u} u_l\phi_l\cdot\nabla\phi_i+div\,\tau(D(\phi_i))\right)\right)\quad\forall\, i,j=1,\dots,N_u.$$

Similarly, we define the pressure term $(B^T+\mathcal{B})\mathbf{P}$ where

$$[B^T]_{i,j}=\int_\Omega\psi_j div\,\phi_i\quad\forall\, i=1,\dots,N_u;\ j=1,\dots,N_p$$

$$[\mathcal{B}]_{i,j}=\sum_{K\in\mathcal{T}_h}\int_K\nabla\psi_j\cdot\left(\delta\int_\Omega\left(\sum_{l=1}^{N_u} u_l\phi_l\cdot\nabla\phi_i+div\,\tau(D(\phi_i))\right)\right)\quad\forall\, i=1,\dots,N_u;\ j=1,\dots,N_p$$

as for $\mathcal{L}_h^2$, we consider

$$\sum_{E\in\Omega^E}\int_{\Omega^E}\left(\frac{1}{\lambda}p_h,q_h\right)$$

which, by replacing p_h by its corresponding finite approximation, gives

$$\sum_{k=1}^{N_p} p_k\sum_{K\in\tau_h}\int_K\frac{1}{\lambda}\psi_i\psi_k=0\quad\forall i=1,\dots N_p.$$

Hence, adding the discretized terms of $\mathcal{L}_1$ and $\mathcal{L}_2$, system (8) becomes

$$\begin{cases}(Q+\mathcal{Q})(\mathbf{U})+(N(\mathbf{U})+\mathcal{N}(\mathbf{U}))\mathbf{U}+(B^T+\mathcal{B})\mathbf{P}=F\\ BU=\mathcal{B}_1\mathbf{P}.\end{cases}\tag{9}$$

As for the cost function (3), we assume that $\mathbf{V}_h$ is associated to a partition $\mathcal{T}_h$ of the domain Ω so that some of the basis functions $(\phi_i)_{i=1\dots N_o}$ can be associated to the nodes on Ω_{part} and some others to the nodes on Γ_{in}, which we denote by $(\phi_i)_{i=1\dots N_g}$. Hence, similarly to $\mathbf{u}_h$, the approximated control function is defined by

$$\mathbf{g}_h=\sum_{j=1}^{N_g} g_j\phi_j\,,$$

where the coefficients g_j correspond to the velocity coefficients u_j associated to Γ_{in}.

To discretize the first term we replace both $\mathbf{u}$ and $\mathbf{u}_d$ by their respective finite dimensional approximations $\mathbf{u}_h$ and $\mathbf{u}_{d,\,h}$. The later is given by

$$\mathbf{u}_{d,h} = \sum_{i=1}^{N_o} u_{d_i}\phi_i\,.$$

Them, we obtain

$$\begin{aligned}
&\int_{\Omega_{\text{part}}} \left\langle \sum_i^{N_o}(u_i - u_{di})\phi_i,\ \sum_j^{N_o}(u_j - u_{dj})\phi_j \right\rangle dx \\
&= \int_{\Omega_{\text{part}}} \sum_i^{N_o}(u_i - u_{di}) \sum_j^{N_o}(u_j - u_{di})\langle \phi_i, \phi_j\rangle\, dx \\
&= \sum_i^{N_o}(u_i - u_{di}) \sum_j^{N_o}(u_j - u_{di}) \int_{\Omega_{\text{part}}} \phi_i\phi_j\, dx \\
&= (U - U_d)^T\mathbf{M}(U - U_d) = \langle (U - U_d), \mathbf{M}(U - U_d)\rangle \\
&= (U - U_d, U - U_d)_M = \|U - U_d\|^2_{N_o}
\end{aligned} \tag{10}$$

where $\|\cdot\|_{N_o}$ is the norm induced by the inner product $(\cdot,\cdot)_M$ and $\mathbf{M}$ is a symmetric $N_o \times N_o$ matrix with general term given by

$$m_{ij} = \int_{\Omega_{\text{part}}} \phi_i\phi_j\, dx\,.$$

Finally, for the regularization term we have

$$\begin{aligned}
&\int_{\Gamma_{in}} \left| \sum_i^{N_g} g_i \nabla\phi_i \right|^2 dx = \int_{\Gamma_{in}} \left\langle \sum_i^{N_g} g_i\nabla\phi_i, \sum_j^{N_g} g_j\nabla\phi_j \right\rangle dx \\
&= \sum_i^{N_g} g_i \sum_j^{N_g} g_j \int_{\Gamma_{in}} \nabla\phi_i : \nabla\phi_j = G^T\mathbf{A}G \\
&= \langle G, \mathbf{A}G\rangle = (G, G)_A = \|G\|^2_{N_g}
\end{aligned} \tag{11}$$

where $\|\cdot\|_{N_g}$ is the norm induced by the inner product $(\cdot,\ \cdot)_A$ and $\mathbf{A}$ is a symmetric $N_g \times N_g$ matrix whose elements are defined by

$$a_{ij} = \int_{\Gamma_{in}} \nabla\phi_i\nabla\phi_j\, dx\,.$$

Taking into account (9)–(11), the discrete version of the control problem (3)–(4) becomes

$$J(U, G) = w_1\|U - U_d\|^2_{N_o} + w_2\|G\|^2_{N_g} \tag{12}$$

subject to (9). We remark that vector $U = (U_g, G)$ includes the controlled velocity coefficients G and the uncontrolled ones $U_g = U_g(G)$.

3.1. Sequential Quadratic Programming (SQP)

Before explaining the method that we have used to solve the nonlinear problem (9)–(12), we first remark that, if we take $F(G) = J(U(G), G)$, it can be written in the general form

$$\min_G F(G) \tag{13}$$

$$H(G) = 0, \tag{14}$$

where (14) represents the problem constraints given by (9) and the Dirichlet boundary conditions.

In what follows we shall also assume that the solution G of (13)–(14) verifies the Karush-Kuhn-Tucker (KKT) optimality conditions

$$DH(G)^T\lambda = DF(G)$$

$$H(G) = 0$$

Table 1
Parameters used in Carreau and Generalized Cross viscosity models.

Model	Parameters
Generalized Cross	$\mu_0 = 0.16\,Pa.s;\ \mu_\infty = 0.0036\,Pa.s;\ \lambda = 8.2\,s;\ a = 1.23;\ b = 0.64$
Carreau	$\mu_0 = 0.0456\,Pa.s;\ \mu_\infty = 0.0032\,Pa.s;\ \lambda = 10.03\,s;\ n = 0.344$

DF and DH are the gradients of F and H, respectively, and λ is the vector of the Lagrange multipliers.

Under these assumptions, we can now apply the SQP version described in [19] whose algorithm can be summarized as follows:

- Consider (G_k, λ_k) to be a fixed estimate for the solution and the corresponding Lagrange multipliers.
- Determine a quasi-Newton approximation $\mathcal{H}_k$ for the Hessian of the modified Lagrangian

$$\mathcal{L}(G, G_k, \lambda_k) = F(G) - \lambda_k^T[H(G_k) - G_k - DH(G_k)(G - G_k)].$$

- Solve the auxiliary Linear Quadratic problem

$$\begin{aligned} &\min_C \mathcal{Q}(G, G_k, \lambda_k) = \\ &= F(G_k) + DF^T(G_k)(G - G_k) - \frac{1}{2}(G - G_k)^T\mathcal{H}_k(G - G_k) \\ &G_k + DH(G_k)(G - G_k) \geq 0 \end{aligned} \tag{15}$$

  to obtain the auxiliary iterate $(\bar{G}_k, \bar{\lambda}_k, \bar{s}_k)$, where $\hat{s}_k$ is the vector of the slack variables associated to the linear constraints in (15).
- Compute $\alpha_{k+1} \in (0, 1]$ as the minimizer of the merit function

$$M_\gamma(G, \lambda, s) = F(G) + \lambda^T(H(G) - s) + \frac{1}{2}\sum_{i=1}^{m}\gamma_i(H_i(G) - s_i)^2$$

  along the line

$$d(\alpha) = (G_k, \lambda_k, s_k) + \alpha[(\bar{G}_k, \bar{\lambda}_k, \bar{s}_k) - (G_k, \lambda_k, s_k)],$$

  where s_i, for $i = 1...m$, are the components of s and γ is a vector of penalty parameters (see [19] for details on the choice of γ). Then set

$$(G_{k+1}, \lambda_{k+1}, s_{k+1}) = d(\alpha_{k+1}).$$

- As a stopping criteria, verify if the optimality tolerance for the KKT conditions is satisfied.

  It is shown in [19] that the sequence $(G_k)_k$ should converge to the solution of the KKT conditions.

4. Numerical results

In this section we present the numerical results that were achieved while trying to validate the Data Assimilation approach described in the previous sections.

In order to be able to obtain a precise indicator of robustness, after fixing the computational domains, we have synthetically generated the known data $\mathbf{u}_d$. This was done by solving the direct (or forward) problem with fixed boundary conditions and parameters.

For the idealized geometries, we have adopted the Generalized Cross viscosity model for blood flow. As to the realistic geometries describing an aneurysm and a bypass, we used the Carreau viscosity model. The specific parameters considered for these two models are presented in Table 1. For the Generalized Cross, the parameters used were chosen as in [30] and [9]. For the Carreau model we followed [36]. In both cases, $\rho = 1050\,\mathrm{Kg/m^3}$ was used as the blood density.

To generate the synthetic data, system (4) was solved, by imposing a Poiseuille velocity profile at the inlet. To this end, we discretized the equations using stabilized P1-P1 finite elements, as described in Section 3. The realistic geometries were obtained by segmentation from medical images. The meshing and assembling of the matrices in (9) were done using COMSOL Multiphysics features [13]. The Newton's method was used to solve the nonlinear problem and, for each resulting linear system, the direct solver PARDISO was used.

Concerning the DA method, there are two factors that contribute to increase its performance: the observed domain Ω_{part} and the weighting parameters w_1 and w_2 that we can choose for each term of the cost function (3). In fact, choosing the observed domain properly, the accuracy of the solution increases (see [11,17,26]). Besides, the correct choice of the cost function parameters can also improve significantly the results (see [24]).

Several experimental tests with the different proposed geometries were executed to find an acceptable choice of parameters. The results have shown that $(w_1, w_2) = (10^4, 10^{-3})$ provides a quite good approximation of the data, including the

Table 2
Straight channel: errors relative to $\mathbf{u}_d$ for both $\mathbf{u}_Q$ and the controlled solution $\mathbf{u}$.

Errors	$\mathbf{u}_Q$	$\mathbf{u}$
AE_Ω	3.439291×10^{-6}	2.477860×10^{-7}
RE_Ω	0.121582	0.009033
$RE_{\Omega_{part}}$	0.043068	0.008986
Cost function	–	1.525862×10^{-5}

velocity and the inlet profile, represented by the optimal control variable. We remark that, when considering $w_2 = 0$, the control variable becomes meaningless as it develops intensive oscillations which correspond to spurious minima of the finite dimensional optimization problem. This was already confirmed in [24] for 2D geometries and, for the sake of brevity, we will not include these results here. We will present here a comparison between different sets of parameters for the examples devoted to realistic geometries.

As described in Section 3.1, each discretized problem of type (9)–(12) was solved by using the SQP method implemented in SNOPT. This method requires the solution of a Linear Quadratic Problem at each iteration, which was obtained using the package SQOPT (see [21]). The gradient of the cost function with respect to the control variables *DF* was computed using the formula

$$DF = \Lambda^T \frac{\partial N}{\partial G} + \frac{\partial F}{\partial G}$$

where the adjoint variable $\Lambda \in R^{N_u}$ is the solution of the adjoint system

$$\frac{\partial N}{\partial U}\Lambda = \frac{\partial F}{\partial U}.$$

In the above expressions, the jacobian matrices $\frac{\partial N}{\partial (.)}$ an $\frac{\partial F}{\partial (.)}$, with respect to both variables U and G, are computed using the symbolic differentiation tool from Comsol Multiphysics [12]. The optimality tolerance, which determines the accuracy of the approximation of the first-order optimality conditions [20], was fixed as 10^{-7} for all cases, except for the aneurysm case, where we choose 10^{-5}.

To analyze the results, we computed the relative and absolute errors between the controlled solution $\mathbf{u}$ and the synthetic solution $\mathbf{u}_d$. These errors are given by

$$RE = \frac{\|\mathbf{u} - \mathbf{u}_d\|_2}{\|\mathbf{u}_d\|_2} \quad \text{and} \quad AE = \|\mathbf{u} - \mathbf{u}_d\|_2,$$

where $\|\cdot\|_2$ is the $\mathbf{L}^2$ norm computed on Ω and Ω_{part}.

4.1. Numerical results in a straight channel

As a first example, and in order to get a clear intuition in the simplest case, we considered an idealized straight channel, with realistic physiological dimensions, as represented on the left of Fig. 3. Hence, we took the length to be equal to $L = 10R$ and the diameter given by $D = 2R$, with $R = 3.1$mm. To verify the algorithm for the model solver, we have used the method of manufactured solutions. We considered the analytic solution

$$\begin{cases} \bar{\mathbf{u}} = \left(0, 0, U_0(1 - (\frac{x}{R})^2 - (\frac{y}{R})^2)\right) \\ \bar{p} = U_0(\frac{0.2}{R} - 0.02\frac{z}{R^2}) \end{cases}$$

with $U_0 = 0.0993$. From this expression, we used the symbolic differentiation tool from Comsol Multiphysics to determine the force vector $\mathbf{f}$ and boundary conditions such that $(\bar{\mathbf{u}}, \bar{p})$ will be the solution of problem (5). Subsequently, we constructed 5 meshes corresponding to a decreasing maximum mesh size, and we used the discretization (9) to solve the problem. Numerical simulations were performed in a quarter part of the channel and the results were extended to the whole domain by symmetry. The relative errors, in the L^2 norm, are presented in Fig. 2. We can see that the convergence is as expected.

Next, we generated the solution to be considered as synthetic data. A mesh corresponding to 330117 degrees of freedom (DOFS) for the velocity, was chosen. The data set, Ω_{part}, is represented by the blue sections across the domain, as we can see in Fig. 3, on the right-hand side. The synthetic solution $\mathbf{u}_d$ was obtained by imposing a parabolic profile at the inlet (Poiseuille profile) corresponding to an inflow rate of $Q = 1.499 \times 10^{-6}\,\text{m}^3/\text{s}$, and a maximum velocity given by $U_0 = 0.0993\,\text{m/s}$.

The control problem (3)–(4) was discretized into the form (9)–(12) using the same mesh and finite elements, and taking 1465 DOFS for the control variable.

The results were analyzed using the errors *RE* and *AE* as criteria. The error *RE* was computed both in the whole domain Ω and in the region Ω_{part}, where the data was assumed to be known. In Table 2 we compare the efficiency of the controlled solution with an alternative solution $\mathbf{u}_Q$ obtained under the assumption that the flow rate, at the inlet, is exactly known. To

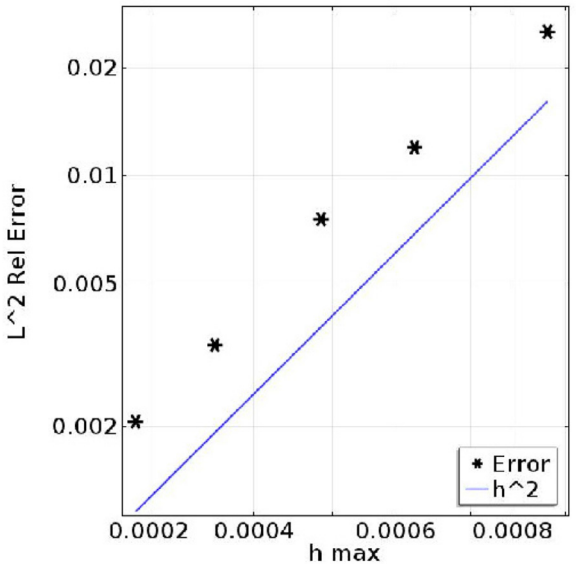


Fig. 2. Mesh convergence with respect to manufactured solution. Relative errors in the L^2 norm. Axis in Log scale.

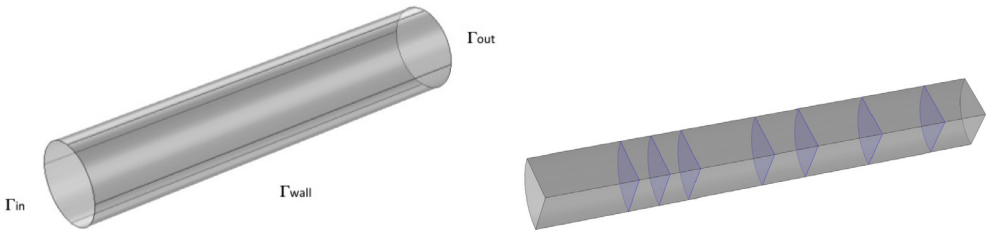


Fig. 3. Left: channel. Right: computational domain and data domain Ω_{part}.

Table 3
Straight channel: errors obtained for different Ω_{part} choices.

Errors	All sections	First section	Last section
AE_{Ω}	2.47786×10^{-7}	1.666634×10^{-6}	1.665239×10^{-6}
RE_{Ω}	0.009033	0.060783	0.060734
$RE_{\Omega_{\text{part}}}$	0.008986	0.059523	0.060193
Cost function	1.525862×10^{-5}	1.445162×10^{-5}	1.449103×10^{-5}

compute such solution, (9) was solved using, as an inflow condition, a constant velocity profile corresponding to the exact flow rate Q. The errors presented in the table measure the difference between each solution $\mathbf{u}$ and $\mathbf{u}_Q$ with respect to $\mathbf{u}_d$. They clearly indicate that the controlled problem has a better performance when recovering the data solution.

In order to understand the role of the location and number of data sections, we performed several numerical tests considering different locations and number of sections. In Table 3, we present the results obtained by considering the observations located only at one section, either close to the inlet, or closer to the outlet. These results are compared, with the ones obtained considering the original Ω_{part} (first column). As expected, the error are smaller when Ω_{part} is constituted by all sections, than when considering only one section. Moreover, in the later case, it is preferable to take a section closer to the outlet.

To illustrate how the controlled solution recovers the synthetic data, we represent in Fig. 4 the velocity magnitude along the working domain. We can verify that the maximum of the velocity is better recovered when all the sections are used for collecting data.

4.2. Numerical results for a curved channel

In this section we present the results obtained for a slightly more complicated geometry consisting of a curved channel. The goal is to understand how the DA assimilation procedure performs under the introduction of a curvature in the geometry. The length of channel along the outer curve is 39.41 mm and along the inner curve is 29.67 mm. The diameter is

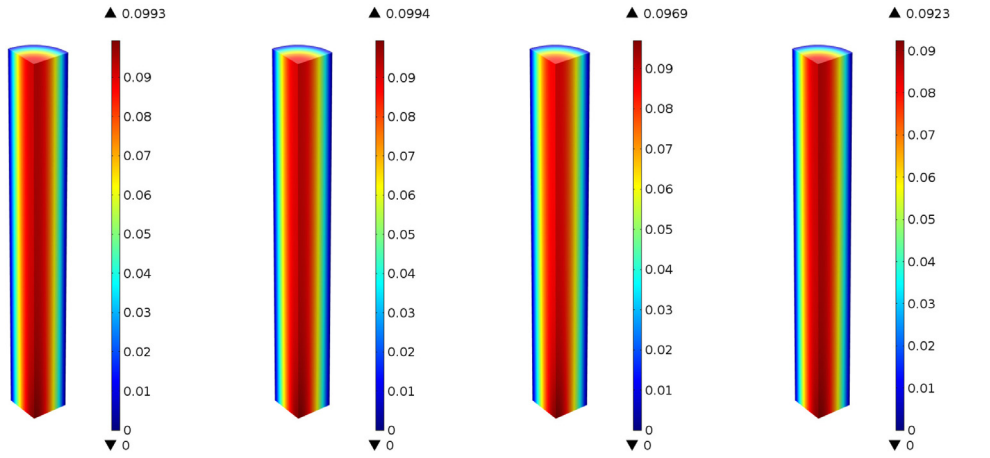


Fig. 4. Channel: velocity magnitude.

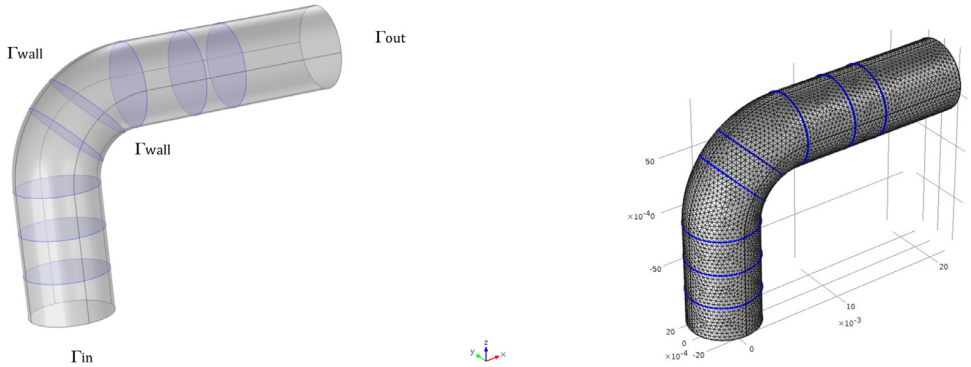


Fig. 5. Left: Curved channel: computational domain with Ω_{part} represented by the blue cross sections. Right: the mesh corresponding to 325695 DOFS.

Table 4
Curved Channel: errors relative to $\mathbf{u}_d$ for both $\mathbf{u}_Q$ and the controlled solution $\mathbf{u}$.

Errors	$\mathbf{u}_Q$	$\mathbf{u}$
AE_Ω	1.310652×10^{-5}	4.458813×10^{-7}
RE_Ω	0.116182	0.005002
$RE_{\Omega_{\text{part}}}$	0.099756	0.005509
Cost function	—	6.066413×10^{-5}

kept as $D = 2R$ with $R = 3.1$ mm. The set Ω_{part} consists of the circular blue sections across the channel and the mesh was constructed taking 325695 DOFS. The geometric representation of the domain is given in Fig. 5.

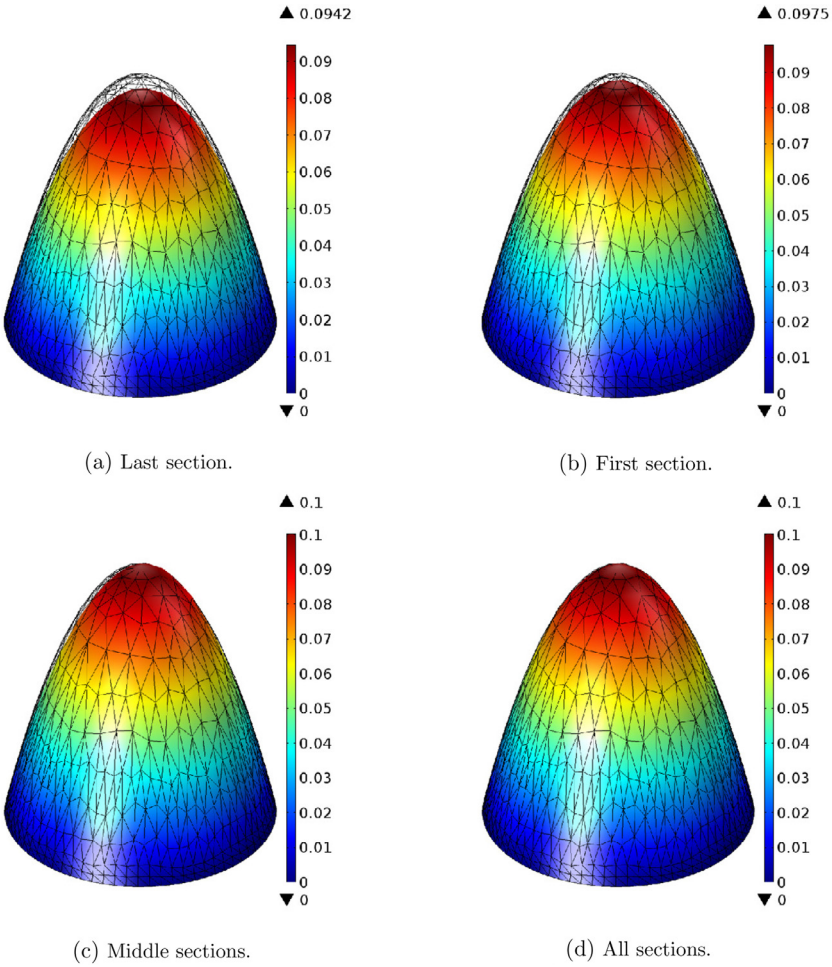
To generate the synthetic data, we used the same inlet velocity profile as for the straight channel. In particular, the same maximum velocity U_0 and flow rate Q were considered.

The control problem was solved with the mesh used for the forward problem and the control variable was discretized with 2337 DOFS. The parameters (w_1, w_2) were kept the same. As done before, we present the errors for $\mathbf{u}$, obtained with all sections in Ω_{part}, and compare them with the errors for $\mathbf{u_Q}$ (see Table 4). The conclusions are similar to the ones obtained for the straight channel.

The results in Table 5 correspond to the same type of tests as those of Table 3. Besides, we also considered the role of the two middle sections (in the curved region), to understand the influence of the channel's curvature. We can see that choosing the middle sections in the curved region improves the accuracy, when compared to the first or last sections choices. Once more, the results indicate that the larger the number of sections, the lower the errors are. Moreover, in Fig. 6, we present the control adjustment to the synthetic data at the inlet. The illustrations are consistent with the results of Table 5.

Table 5
Curved channel: errors obtained for different Ω_{part} choices.

Errors	All sections	First section	Middle sections	Last section
AE_{Ω}	4.458813×10^{-7}	2.813992×10^{-6}	1.66500×10^{-6}	3.428682×10^{-6}
RE_{Ω}	0.005002	0.031827	0.018935	0.039623
$RE_{\Omega_{\text{part}}}$	0.005509	0.045608	0.022044	0.0064
Cost function	6.066413×10^{-5}	5.819608×10^{-5}	5.939748×10^{-5}	5.762889×10^{-5}



(a) Last section. (b) First section.

(c) Middle sections. (d) All sections.

Fig. 6. Curved channel: control adjustment considering Ω_{part} as the last section (a), the first section (b), only the middle (curvature) sections (c), and all sections (d). The synthetic (desired) solution is represented using black wireframe. The controlled solution **u** is represented with color scale.

4.3. Numerical results for a bypass

The great interest of this methodology is the possibility of its application to real clinical situations, which demands being reliable for clinical practice. At this stage, the goal remains to perceive what happens when real geometries are considered, even if synthetically generated data is used. Following this direction, we apply the proposed Data Assimilation approach to a computational domain representing the region of an artery including a bypass junction. The geometry was obtained from a Magnetic Resonance Imaging (MRI) data set. After segmentation, a NURBS based parametrization was used to define the domain. The resulting computational domain is represented in Fig. 7.

To generate the synthetic solution, we used the same type of finite elements, with 372636 DOFS. At the inlet, we imposed, once more, a parabolic profile corresponding to a flow rate of $Q = 4 \times 10^{-6}\,\text{m}^3/\text{s}$, a Reynolds number of $Re = 355$ and a maximum velocity of $U_0 = 0.378788\,\text{m/s}$. As to Γ_{out}, although in this case it consists of two boundaries, we have still imposed a homogeneous Neumann boundary condition. This choice is clearly not representative of the pulsatile flow arising in such type of pathological situation, but it serves the purpose of testing our method in different 3D models, with realistic Reynolds numbers and computational domains. In Fig. 8(a) we represent the velocity streamlines for this synthetic solution.

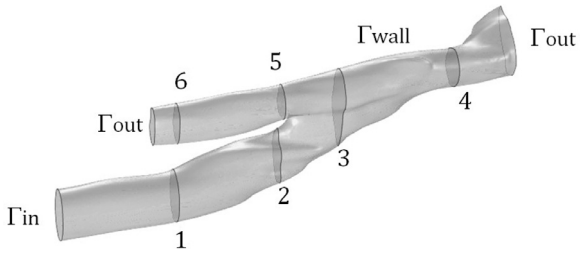


Fig. 7. Bypass: computational domain.

Table 6
Bypass: errors relative to $\mathbf{u}_d$ for $\mathbf{u}_Q$ and the controlled solutions $\mathbf{u}$, for both sets of parameters $p_1 = (10^3, 10^{-3})$ and $p_2 = (10^4, 10^{-3})$.

Errors	$\mathbf{u}_Q$	Weights	$\mathbf{u}$
AE_Ω	3.16013×10^{-5}	p_1	3.948×10^{-5}
		p_2	7.9153×10^{-6}
RE_Ω	0.122	p_1	0.15241
		p_2	0.03056
$RE_{\Omega_{part}}$	0.099241	p_1	0.151772
		p_2	0.021544
Cost function	—	p_1	9.385×10^{-4}
		p_2	1.1×10^{-3}

Table 7
Bypass: errors obtained for different Ω_{part} choices, using parameters $p_2 = (10^4, 10^{-3})$.

Weight	Errors	All sections	All sect. except 4	All sect. except 5 & 6
p_2	AE_Ω	7.9153×10^{-6}	8.7601×10^{-6}	7.9740×10^{-6}
	RE_Ω	0.03056	0.03382	0.03079
	$RE_{\Omega_{part}}$	0.021544	0.026353	0.021815
	Cost function	1.1×10^{-3}	1.1×10^{-3}	1.1×10^{-3}

For the DA approach, we considered Ω_{part} as the set of cross sections represented in Fig. 7. The discretization of the control problem is based on the same finite elements used for the synthetic data. The control variable was discretized with 382 DOFS. We tested different parameter pairs for the cost functional (w_1, w_2). Here, we present the results for two significant pairs, $p_1 = (10^3, 10^{-3})$ and $p_2 = (10^4, 10^{-3})$. The objective is to highlight the improvement of the results as the weight, assigned to the data misfit term, increases.

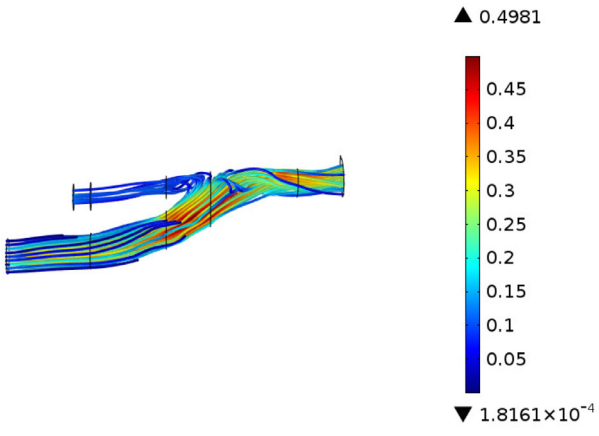
Similarly to the previous cases, we also compare the controlled solution with the solution $\mathbf{u}_Q$, obtained by solving (9) using a constant velocity (averaged from the flow rate Q) at the inlet (see Fig. 8 (c)). Therefore, when comparing $\mathbf{u}$ and $\mathbf{u}_Q$, the differences do not depend on the flow rate, but rather on the velocity profile itself.

In Table 6 we present the computed errors between the synthetic solution $\mathbf{u}_d$ and both $\mathbf{u}_Q$, and the controlled solution $\mathbf{u}$.

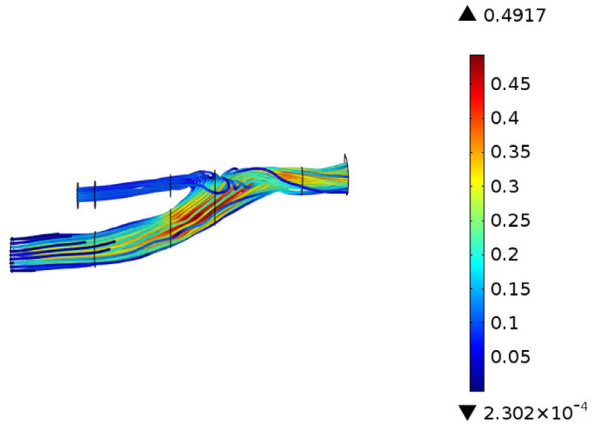
Comparing the results for the weighting parameters p_1 and p_2, it is clear that a higher w_1 provides lower error values and, consequently, better optimization results. We represent the optimized solution associated to a lower relative error in Fig. 8(b). In Fig. 9(a), (c) and (e) the relative error between the data and the controlled solution is represented on sections 2, 3, and 5. It can be directly compared with the same error with respect to solution $\mathbf{u}_Q$, obtained from the exact flow rate Fig. 9(b), (d) and (f). The results indicate that the relative error can be reduced down to one-fifth, when using the DA procedure.

We have also performed several numerical tests, where the sections in Ω_{part} have been changed, to identify the best location to collect data in order to obtain more accurate results. Observing Table 7, we see that the errors obtained in the case when all sections are considered, and those obtained when sections 5 and 6, are removed, are very similar. When considering all sections except section 4, we can see that the error is significantly higher. From these results, it is possible to conclude that cross sections 5 and 6 could be omitted in the numerical simulations. However, the same does not happen with section 4, for which a larger error indicates that this cross-section should be considered an important one. This is an expected result, since the cross sections 5 and 6 belong to a region where the flow rate is lower, and the velocity profile doesn't change significantly (see Fig. 8(a)).

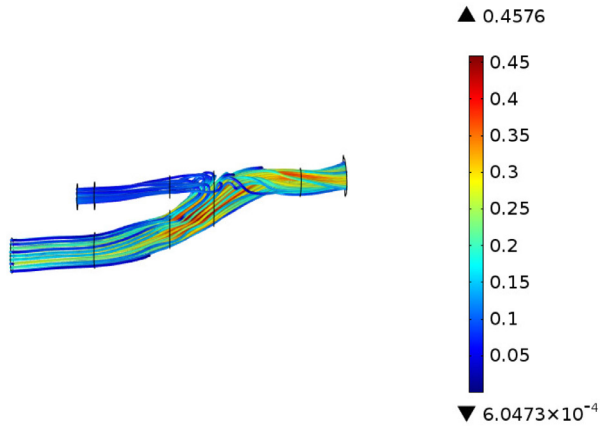
Fig. 10 represents the control adjustement to the parabolic inlet velocity used to generate the synthetic data $\mathbf{u}_d$. We compare the results for both set of parameters p_1 (Fig. 10 (a)) and p_2 (Fig. 10 (b)), considering all data sections. The best adjustment (Fig. 10 (b)) is obtained with the parameters p_2, consistently with Table 6.



(a) $\mathbf{u}_d$.



(b) $\mathbf{u}$, all sections, p_2.



(c) $\mathbf{u}_Q$.

Fig. 8. Bypass: streamlines for $\mathbf{u}_d$, controlled solution $\mathbf{u}$ (obtained with data from all sections) and flow rate based solution $\mathbf{u}_Q$.

To verify that the previous conclusions were not a result of the so called *inverse crime*, we also performed several experiments adding noise to the data observations. The noise was generated by adding to the synthetic solution, in Ω_{part}, a perturbation randomly generated. The noise was therefore picked along the normal distribution with zero mean and standard deviation given by $\bar{\sigma} = V\frac{U_0}{3}$. In this formula, U_0 represents the maximum velocity of $\mathbf{u}_d$ measured at the inlet boundary and $V \in \{0.1, 0.2, 0.4\}$. Such experiments are considered more realistic as, in real situations, data measurements are subject to the inherent noise associated with measurement devices. Table 8, shows the relative errors computed for both cases p_1

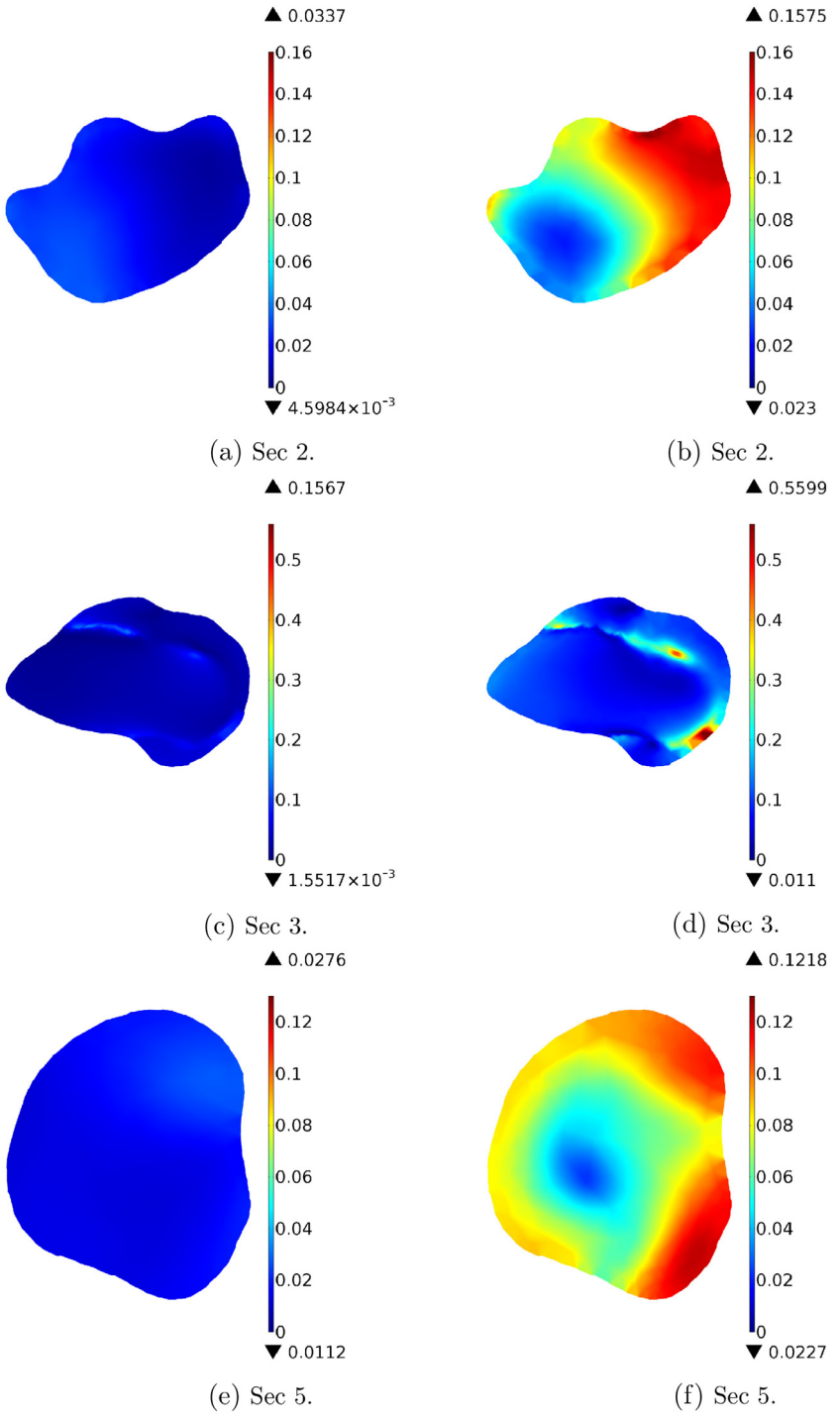
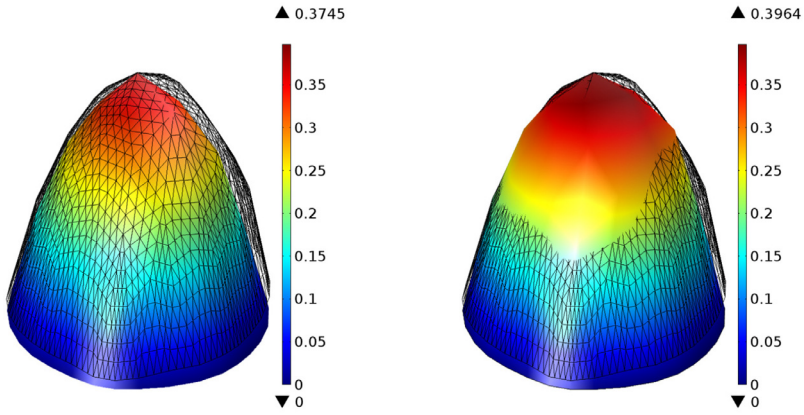


Fig. 9. Bypass: plots of the relative errors between $\mathbf{u}_d$ and $\mathbf{u}$ (left column), $\mathbf{u}_d$ and $\mathbf{u}_q$ (right column), represented in Sections 2, 3 and 5.

and p_2, and different values of V. The low relative errors confirm what has been suggested in [18] and [24], where it was shown that the variational DA approach can be robust to noisy data.

Finally, we present numerical results for the case where, besides Γ_{in}, we also control one of the outflow boundaries. We chose the outflow boundary adjacent to cross-section 6, represented in Fig. 7. Since the regularization term has now a different weight in the cost function, new set of parameters were tested. In Table 9, we present the relative errors for the parameters $p_1 = (10^3, 10^{-3})$, $p_2 = (10^4, 10^{-3})$ and $p_3 = (10^5, 10^{-3})$. It can be seen that, even in case of two controlled



(a) All sections, p_1. (b) All sections, p_2.

Fig. 10. Bypass: control adjustment considering the parameters in the cost functional as $p_1 = (10^3, 10^{-3})$ (a), and $p_2 = (10^4, 10^{-3})$ (b). The synthetic (desired) solution is represented using black wireframe. The controlled solution $\mathbf{u}$ is represented with color scale.

Table 8
Bypass: relative errors computed in Ω_{part} obtained by including noise in the data, for both pair of parameters p_1 and p_2.

Errors	Noise	Weights	$\mathbf{u}$
$\text{RE}_{\Omega_{\text{part}}}$	10%	p_1	0.151756
		p_2	0.021476
	20%	p_1	0.15176
		p_2	0.021986
	40%	p_1	0.153731
		p_2	0.023047

Table 9
Bypass: control of two artificial boundaries. Relative errors of $\mathbf{u}$ with respect to $\mathbf{u}_d$, for both sets of parameters p_2 and p_3.

Errors	$\mathbf{u}_Q$	Weights	$\mathbf{u}$
AE_Ω	3.16013×10^{-5}	p_1	9.96291×10^{-4}
		p_2	8.9355×10^{-6}
		p_3	4.3118×10^{-6}
RE_Ω	0.122	p_1	0.17056
		p_1	0.03056
		p_3	0.01699
$\text{RE}_{\Omega_{\text{part}}}$	0.099241	p_1	0.17644
		p_2	0.02748
		p_3	0.00419
Cost function	–	p_1	9.96291×10^{-4}
		p_2	1.25×10^{-3}
		p_3	1.3×10^{-3}

boundaries, the Data Assimilation procedure can substantially reduce the relative errors comparatively to the solution $\mathbf{u}_Q$, obtained from a known flow rate at Γ_{in}.

4.4. Numerical results for a cerebral aneurysm

As a last test case, we chose another realistic geometry representing an artery with a saccular cerebral aneurysm of saccular type. The 3D geometry was obtained by segmentation of Computed Tomography (CT) data sets (Fig. 11). To generate $\mathbf{u}_d$ we used a mesh corresponding to 138480 DOFS. Again, a parabolic profile was used, characterized by a Reynolds number of $Re = 373$ (flow rate of $Q = 4 \times 10^{-6}\, m^3/s$) and a maximum inlet velocity $U_0 = 0.419507$ (see Fig. 12(a) and (b)).

To solve the DA problem, we considered Ω_{part} to be the set represented by the circular blue sections in Fig. 11. As in the bypass case, we show the results for the pairs of parameters $p_1 = (10^3, 10^{-3})$, $p_2 = (10^4, 10^{-3})$. The control variable was discretized using 376 DOFS. The controlled solution, obtained with the parameters p_2, is represented in Fig. 12 (c) and (d). In Fig. 12(e) and (f), we represent the solution $\mathbf{u}_Q$, generated, once more, using the exact flow rate. We observe that the

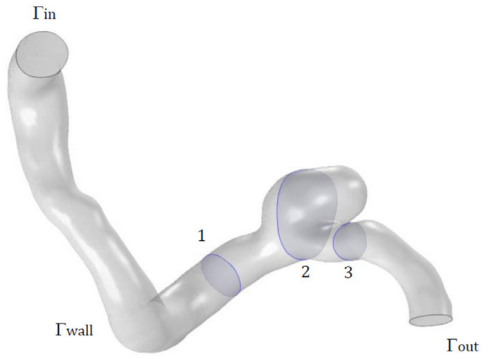


Fig. 11. Aneurysm: computational domain.

Table 10
Aneurysm: errors relative to $\mathbf{u}_d$ for $\mathbf{u}_Q$ and the controlled solutions $\mathbf{u}$, for both sets of parameters p_1 and p_2.

Errors	$\mathbf{u}_Q$	Weights	$\mathbf{u}$
AE_Ω	3.72217×10^{-5}	p_1	6.704×10^{-5}
		p_2	1.358×10^{-5}
RE_Ω	0.08921	p_1	0.17905
		p_2	0.03628
$RE_{\Omega_{part}}$	0.026335	p_1	0.185767
		p_2	0.022283
Cost function	–	p_1	1.14×10^{-3}
		p_2	1.37×10^{-3}

Table 11
Aneurysm: errors obtained for different Ω_{part} choices, using parameters $p_2 = (10^4, 10^{-3})$.

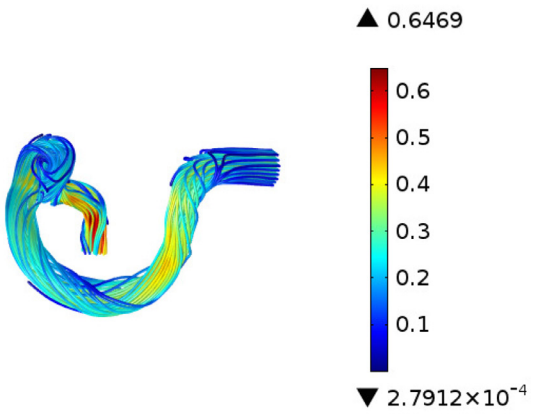
Weight	Errors	All sec.	Sec 1	Sec 2	Sec 3
p_2	AE_Ω	1.358×10^{-5}	3.722171×10^{-5}	2.035765×10^{-5}	2.389161×10^{-5}
	RE_Ω	0.03628	0.099413	0.054372	0.063811
	$RE_{\Omega_{part}}$	0.022283	0.097367	0.04874	0.062141
	Cost function	1.37×10^{-3}	0.001263	0.001329	1.380.001314

Table 12
Aneurysm: relative errors computed in Ω_{part} obtained by including noise in the data, for both parameters pairs p_1 and p_2.

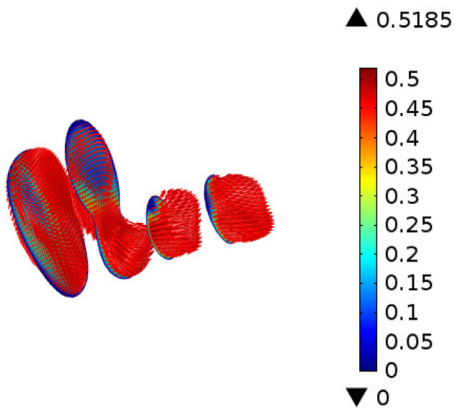
Errors	Noise	Weights	$\mathbf{u}$
$RE_{\Omega_{part}}$	10%	p_1	0.186083
		p_2	0.02251
	20%	p_1	0.186106
		p_2	0.022336
	40%	p_1	0.185373
		p_2	0.021369

assimilated solution $\mathbf{u}$ approximates better the synthetic solution, in the whole domain and in terms of maximum velocity magnitudes. When looking at the sections inside and after the aneurysm dome, we see that both the controlled solution and the solution obtained with average velocity (from known flow rate) are quite accurate. As suggested in [33], the fact that this region is located far from the inlet, downstream several geometrical accidents, makes it less sensitive to the inlet profile, as long as the flow rate is fixed. In Table 10 we can confirm that the controlled solution is much more accurate in the whole domain. In Ω_{part}, the difference is not so significant. As with the previous examples, we obtain better results using the pair of parameters p_2.

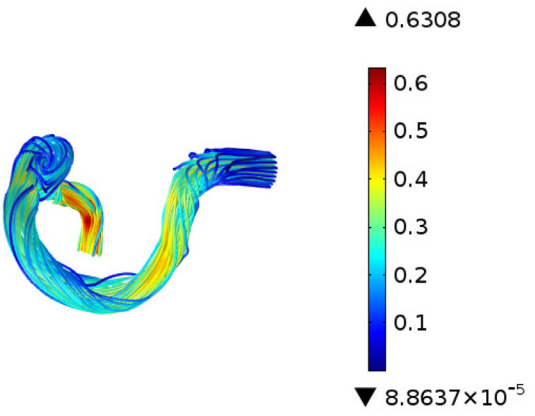
Next, we also present the results comparing different choices for the sections in Ω_{part}. Table 11 shows the results obtained for p_2, considering the three sections, and each one individually. Analyzing the results, it is clear that, as in the previous examples, considering all sections provides lower errors than considering only one section. When using each one of these sections individually, we see that all of them allow to recover the synthetic data accurately. However, using cross Section 2, located inside the aneurysm, gives the lowest errors among the three of them.



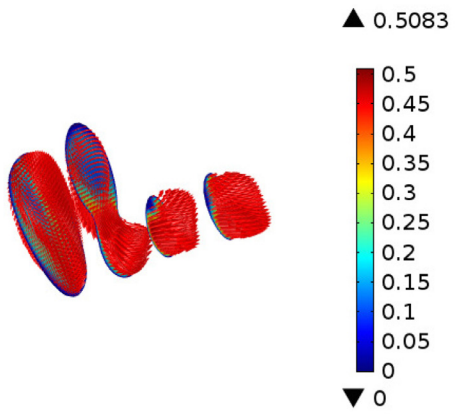
(a) Streamlines for $\mathbf{u}_d$.



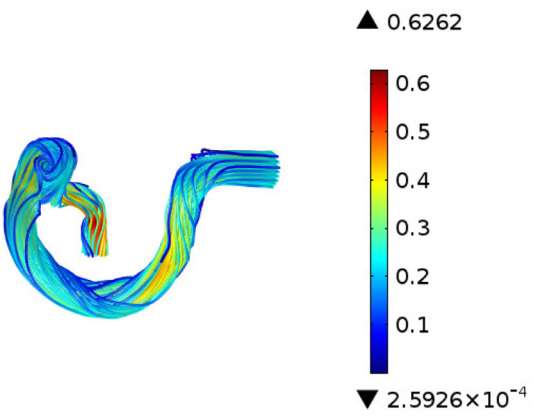
(b) Velocity vectors for $\mathbf{u}_d$.



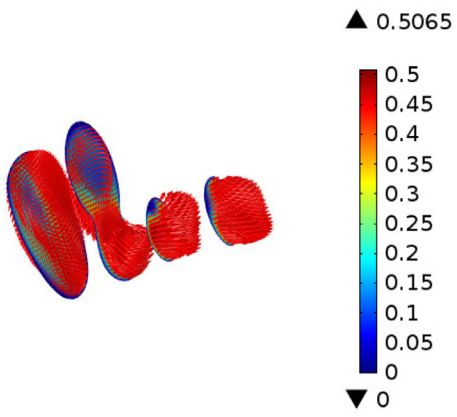
(c) Streamlines for $\mathbf{u}$, all sections, p_2.



(d) Velocity vec. for $\mathbf{u}$, all sections, p_2.



(e) Streamlines for $\mathbf{u}_Q$.



(f) Velocity vectors for $\mathbf{u}_Q$.

Fig. 12. Aneurysm: velocity streamlines for $\mathbf{u}_d$, controlled solution $\mathbf{u}$ and $\mathbf{u}_Q$ (Left). Velocity magnitude and vectors in the aneurysm area for the same solutions (Right).

Finally, in order to check robustness against possible *inverse crimes*, we considered several levels of noise, generated as described in Section 4.3. Once again, the low relative errors indicate that the Data Assimilation procedure was able to recover accurate solutions, with respect to the synthetic solution. These results can be observed in Table 12.

5. Conclusion

We have proposed a Data Assimilation method, based on a Dirichlet control problem, to numerically reconstruct the blood flow profile in 3D realistic geometries, assuming a shear-thinning rheology for blood in the steady case. We have

applied the approach to several examples associated to idealized and realistic computational domains of interest, from the clinical point of view. The data was polluted with noise in order to mimic realistic scenarios.

Using synthetic ground truth solutions, we conclude that the method allows the accurate reconstruction of the velocity profile with a relative error smaller than 2%. Concerning the choice of the regions for data acquisition we have verified that, according to the geometry, different locations can be preferred. In a simple straight channel, performance improves while decreasing the inlet distance. On the other hand, in geometries with different flow structures, locations associated to regions with significant velocity changes seem to be better suited. The results also depended on the choice of the parameters used in the control cost function. While we were able to heuristically find some parameters that would fit in all the examples, a proper quantitative method to adjust such parameters still needs to be defined.

The Data Assimilation method here proposed revealed an accurate alternative to the use of average velocities as an inlet profile. The good results, for the stationary case, motivate a more general procedure, to address data which can be obtained at different moments of the cardiac cycle.

Acknowledgments

This work has been partially supported by FCT (Portugal) through the Research Project UID/Multi/04621/2013 of the CEMAT - Center for Computational and Stochastic Mathematics (at Instituto Superior Técnico, University of Lisbon), the grant SFRH/BPD/66638/2009 and the project EXCL/MAT-NAN/0114/2012.

References

[1] F. Abraham, M. Behr, M. Heinkenschloss, The effect of stabilization in finite element methods for the optimal boundary control of the Oseen equations, Finite Elem. Anal. Des. 41 (2003) 229–251.
[2] N. Arada, Optimal control of shear-thinning fluids, SIAM J. Control Optim. 40 (4) (2012) 2515–2542.
[3] J. Baranger, K. Najib, Analyse numérique des écoulements quasi-newtoniens dont la viscosité obéit à la loi puissance ou la loi de carreau, Numer. Math. 58 (1990) 35–49.
[4] J.W. Barrett, S.W. Liu, Finite element error analysis of a quasi-newtonian flow obeying the Carreau or power law., Numerische Mathematik 64 (1) (1993) 433–453.
[5] Y. Bazilevs, V. Calo, T. Tezduyar, T. Hughes, YZβ discontinuity capturing for advection-dominated processes with application to arterial drug delivery, Int. J. Numer. Meth. Fluids 54 (2007) 593–608.
[6] F. Shakib, T. Hughes, J. Zdenk, A new finite element formulation for computational fluid dynamics: X. the compressible euler and navier-Stokes equations, Comput. Meth. Appl. Mech. Eng. 89 (1991) 141–219.
[7] L. Bertagna, A. Veneziani, A model reduction approach for the variational estimation of vascular compliance by solving an inverse fluid-structure interaction problem., Inverse Prob. 30 (5) (2014) 055006.
[8] J.T. Betts, S.L. Campbell, Discretize Then Optimize, Technical Document series, &CT-TECH-03-01, Mathematics and Computing Technology, Phantom Works, Boeing, Seattle, 2003.
[9] T. Bodnar, A. Sequeira, M. Prosi, On the shear-thinning and viscoelastic effects of blood flow under various flow rates, Appl. Math. Comput. 217 (2011) 5055–5067.
[10] A. Brooks, T. Hughes, Streamline upwind/petrov-galerkin formulations for a convection dominated flows with a particular emphasis on the incompressible navier-stokes equations, Comput. Methods Appl. Mech. Eng. 32 (1982) 199–259.
[11] J. Burkardt, M. Gunzburger, J. Peterson, Insensitive functionals, inconsistent gradients, spurious minima and regularized functionals in flow optimization problems, Int. J. Comput. Fluid Dyn. 16 (3) (2002) 171–185.
[12] COMSOL Multiphysics, Users Guide, COMSOL 4.3, 2012.
[13] COMSOL Multiphysics, http://www.comsol.com.
[14] E. Casas, L.A. Fernandez, Boundary control of quasilinear elliptic equations, Rapport de Recherche, INRIA 782 (1988).
[15] E. Casas, L.A. Fernandez, Distributed control of systems governed by a general class of quasilinear elliptic equations, J. Differ. Equ. 104 (1993) 20–47.
[16] S. Collis, M. Heinkenschloss, Analysis of the streamline upwind/petrov Galerkin method applied to the solution of optimal control problems, Technical Report TR02-01.DCAM Rice University, Houston Tx March, 2002.
[17] M.D. Elia, M. Perego, A. Veneziani, A variational data assimilation procedure for the incompressible Navier-Stokes equations in hemodynamics, J. Sci. Comput. 52 (2) (2011) 340–359.
[18] M. D'Elia, A. Veneziani, Methods for assimilating blood velocity measures in hemodynamics simulations: preliminary results, Procedia Comput. Sci. 1 (1) (2010) 1225–1233.
[19] P. Gill, W. Murray, M.A. Saunders, SNOPT: An SQP algoritm for large-scale constrained optimization, Soc. for Ind. Appl. Math. 47 (2005) 99–131.
[20] P. Gill, W. Murray, M.A. Saunders, User's guide for SNOPT version 7: Software for large-scale nonlinear programming, 2008,
[21] P. Gill, W. Murray, M.A. Saunders, User's Guide for SQOPT Version 7: Software For large-scale linear and quadratic programming, Numerical Analysis Report 06-1, Department of Mathematics, University of California San Diego, La Jolla, CA, 2006.
[22] T. Guerra, Distributed control for shear-thinning non-newtonian fluids, J. Math. Fluid Mech. 14 (4) (2012) 771–789.
[23] T. Guerra, A. Sequeira, J. Tiago, Existence of optimal boundary control for Navier-Stokes with mixed boundary conditions, Port. Math. 72 (2–3) (2015) 267–283.
[24] T. Guerra, J. Tiago, A. Sequeira, Optimal control in blood flow simulations, Int. J. Non-Linear Mech. 64 (2014) 57–59.
[25] M. Gunzburger, Adjoint equation-based methods for control problems in incompressible viscous flows, Flow, Turbul. Combust. 65 (3) (2000) 249–272.
[26] M. Gunzburger, Perspectives in flow control and optimization, in: Advances in Design and Control, SIAM, Philadephia, PA, 2003.
[27] M. Gunzburger, C. Trenchea, Analysis of an optimal control problem for the three-dimensional coupled modified navier-stokes and maxwell equations, J. Math. Anal. Appl. 333 (2007) 295–310.
[28] M. Heinkenschloss, D. Leykekhman, Local error estimates for SUPG solutions of advection-dominated elliptic linear-quadratic optimal control problems, SIAM J. Numer. Anal. 47 (6) (2010) 4607–4638.
[29] M. Hinze, F. Tröltzsch, Discrete concepts versus error analysis in PDE-constrained optimization, GAMM-Mitt 33 (2) (2010) 148–162.
[30] A. Leuprecht, K. Perktold, Computer simulation of non-newtonian effects on blood flow in large arteries, Comput. Meth. Biomech. Biomech. Eng. 4 (2) (2001) 149–163.
[31] A. Marsden, Optimization in cardiovascular modeling, Annual Rev. Fluid Mech. 46 (2014) 519–546.
[32] P. Moireau, C. Bertoglio, N. Xiao, C.A. Figueroa, C.A. Taylor, D. Chapelle, J.-F. Gerbeau, Sequential identification of boundary support parameters in a fluid-structure vascular model using patient image data, Biomech. Model. Mechanobiol. 12 (3) (2013) 475–496.
[33] K.R. Moyle, L. Antiga, D.A. Steinman, Inlet conditions for image-based CFD models of the carotid bifurcation: is it reasonable to assume fully developed flow? J. Biomech. Eng. 128 (3) (2006) 371–379.

[34] S. Pant, B. Fabreges, J.F. Gerbeau, I. Vignon-Clementel, A methodological paradigm for patient-specific multi-scale CFD simulations: from clinical measurements to parameter estimates for individual analysis, Int. J. Numer. Meth. Biomed. Eng. 30 (12) (2014) 1614–1648.
[35] A.M. Robertson, A. Sequeira, G.R. Owens, Rheological models for blood, Cardiovascular Mathematics, Modeling and Simulation of the circulatory system, Springer, Milan, 2009, pp. 211–241.
[36] A.M. Robertson, A. Sequeira, M. Kameneva, Hemorheology. hemodynamical flows, in: Modeling, Analysis and Simulation, 37, Birkhauser Verlag Basel, Switzerland, 2008, pp. 63–120.
[37] T. Slawig, Distributed control for a class of non-newtonian fluids, J. Differ. Equ. 219 (2005) 116–143.
[38] J. Tiago, A. Gambaruto, A. Sequeira, Patient-specific blood flow simulations: setting dirichlet boundary conditions for minimal error with respect to measured data, Math. Models Nat. Phenomena 9 (6) (2014) 98–116.
[39] D. Wachsmuth, T. Roubíček, Optimal control of incompressible non-newtonian fluids, Z. Anal. Anwend 29 (2010) 351–376.
[40] B. Wang, X. Zou, J. Zhu, Data assimilation and its applications., Proc. Natl. Acad. Sci. USA 97 (21) (2000) 11143–11144.